ARTICLE

Application of fluorescent dextrans to the brain surface under constant pressure reveals AQP4-independent solute uptake

Alex J. Smith[1,2] (iD), Gokhan Akdemir[2], Meetu Wadhwa[1], Dan Song[2] (iD), and Alan S. Verkman[2]

Extracellular solutes in the central nervous system are exchanged between the interstitial fluid, the perivascular compartment, and the cerebrospinal fluid (CSF). The "glymphatic" mechanism proposes that the astrocyte water channel aquaporin-4 (AQP4) is a major determinant of solute transport between the CSF and the interstitial space; however, this is controversial in part because of wide variance in experimental data on interstitial uptake of cisternally injected solutes. Here, we investigated the determinants of solute uptake in brain parenchyma following cisternal injection and reexamined the role of AQP4 using a novel constant-pressure method. In mice, increased cisternal injection rate, which modestly increased intracranial pressure, remarkably increased solute dispersion in the subarachnoid space and uptake in the cortical perivascular compartment. To investigate the role of AQP4 in the absence of confounding variations in pressure and CSF solute concentration over time and space, solutes were applied directly onto the brain surface after durotomy under constant external pressure. Pressure elevation increased solute penetration into the perivascular compartment but had little effect on parenchymal solute uptake. Solute penetration and uptake did not differ significantly between wild-type and AQP4 knockout mice. Our results offer an explanation for the variability in cisternal injection studies and indicate AQP4-independent solute transfer from the CSF to the interstitial space in mouse brain.

Introduction

Exchange of solutes between subarachnoid cerebrospinal fluid (CSF) and brain interstitial fluid (ISF) via the perivascular compartment, which has long been recognized, has important implications for brain physiology, pathology, and drug delivery (Abbott, 2004; Bakker et al., 2016; Pizzo et al., 2018). To enter the brain, solutes injected into the CSF initially disperse in the subarachnoid space and then cross the pia or the arterial sheath via pores (stomata) between the leptomeningeal cells (Zervas et al.,1982; Pizzo et al., 2018). Solutes can then be transported deeper into the brain via periarterial spaces and cross the basement membrane and glial endoot layer for entry into the parenchyma (Ichimura et al., 1991; Iliff et al., 2012; Kutuzov et al., 2018; Pizzo et al., 2018). Solutes in the parenchymal interstitial space can be cleared to the subarachnoid space via the periarterial spaces (Albargothy et al., 2018), and possibly the perivenous spaces (Iliff et al., 2012). Controversy exists regarding the barriers to solute uptake by the perivascular pathways, the direction and rate of solute transport in the perivascular compartment, and the relative contributions of diffusive and advective solute transport in the parenchyma (Iliff et al., 2012; Hladky and Barrand, 2014; Smith and Verkman, 2018; Abbott et al., 2018).

The "glymphatic" mechanism (Iliff et al., 2012; Nedergaard 2013) posits that solute exchange between CSF and ISF involves the astrocyte water channel aquaporin-4 (AQP4), which has been proposed to regulate advective flow of CSF through the brain parenchyma from periarterial to perivenular spaces. Modeling studies have reported that the hydraulic resistance of brain parenchyma is far too high for significant advective transport (Jin et al., 2016; Holter et al., 2017). Experimental studies have demonstrated that clearance of interstitial solutes occurs via the periarterial spaces (Albargothy et al., 2018) or the ventricles (Rosenberg et al., 1980; Bedussi et al., 2015) and that injected tracers are not seen surrounding the walls of veins (Carare et al., 2008). Additionally, we showed that solute movement in parenchyma is diffusive and nondirectional (Smith et al., 2017), in agreement with longstanding theories on extracellular transport in brain parenchyma (Syková and Nicholson, 2008).

---

[1]Department of Ophthalmology, University of California San Francisco, San Francisco, CA; [2]Departments of Medicine and Physiology, University of California San Francisco, San Francisco, CA.

Correspondence to Alex J. Smith: alex.smith@ucsf.edu.

Nonetheless, a role for AQP4 in perivascular solute movement is conceivable given its prominent enrichment at the adluminal face of astrocyte endfeet (Verbavatz et al., 1997; Rash et al., 1998).

Experimental studies to investigate the contribution of AQP4 to solute exchange between the CSF and brain interstitium following injection of solutes into the cisterna magna of mice have generated results that diverge widely in both the basal extent of solute uptake and the effect of AQP4 deletion (Iliff et al., 2012; Smith et al., 2017; Mestre et al., 2018a; see Discussion). This experimental variation has been attributed to a variety of factors, including choice of anesthetic, animal background strain, fixation conditions, and other technical factors. Here, we report an additional source of experimental variability: the effect of solution injection conditions, including injection rate and fluid volume, on the temporal and spatial pattern of solute uptake. We found that higher injection rates remarkably enhanced the dispersal of solutes in the subarachnoid space and increased solute uptake at the cortical surface, and that elevated intracranial pressure (ICP) increased perivascular solute uptake. In addition, a novel external constant-pressure approach, which does not suffer from the confounding factors of cisternal injection, clarified the role of pressure on solute delivery from CSF to brain interstitium and provided additional evidence against the involvement of AQP4 in this process.

Materials and methods

Animals
Experiments were performed on wild-type and AQP4 knockout mice (Ma et al., 1997; Manley et al., 2000) bred on a CD1 background at age 6–10 wk. All animal procedures were approved by the University of California, San Francisco Institutional Animal Care and Use Committee.

Materials
Fixable fluorescent dextrans (FITC, 2,000 kD; TRITC, 70 kD; Alexa Fluor 647, 10 kD; Molecular Probes) were dissolved at 10 mg/ml in artificial CSF (aCSF), stored as frozen aliquots at –70°C, and diluted with aCSF to specified concentrations before use. Antibody sources were as follows: CD31 antibody (550274; BD PharMingen), α smooth muscle actin antibody (NB300-97855; Novus Biologicals), and fluorophore-labeled secondary antibodies (Molecular Probes). Other chemicals were from Sigma-Aldrich.

Cisternal injections
Mice were anesthetized with ketamine (100 mg/kg) and xylazine (10 mg/kg) and immobilized on a stereotaxic frame, and the dura overlying the cisterna magna was surgically exposed. Deep anesthesia was maintained throughout the experiments with additional small doses of ketamine as needed. A 30-g needle attached to a syringe pump via polyethylene tubing, which was preloaded with the specified volume and concentration of solutes, was inserted into the cisterna magna and cemented in place with cyanoacrylate glue. In experiments where solutes were chased with aCSF, a small bubble (~0.2 µl) was used to separate the solute solution from the aCSF to prevent mixing. At the end of injections, the tubing was heat cauterized to prevent backflow, and the needle was left in place. Mice remained immobilized on the stereotaxic frame for 25 min after injection and were then removed from the frame and transported to a fume hood for transcardial perfusion fixation. Perfusion was initially with cold, heparinized PBS for 3 min, and then with 4% paraformaldehyde in PBS for a further 12 min. The total interval between the removal of mice from the stereotaxic frame to the arrival of fixative in the brain was estimated at 5 min. After perfusion, brains were removed and placed in 4% paraformaldehyde overnight before sectioning.

Direct solute application to the brain surface
Mice were anesthetized with ketamine and xylazine and immobilized on a stereotaxic frame. A 2–3-mm-diameter parietal hole was cut with a microdrill and carefully removed to expose the dura. The dura was then surgically removed using the tip of a 24-g needle, and a drop of aCSF was placed over the cranial hole to maintain tissue hydration. A 5-ml polystyrene serological pipette, which was trimmed at the end to increase its diameter to ~5 mm, was placed over the hole and cemented in place with cyanoacrylate glue followed by dental cement. 0.5 ml of aCSF containing the three fixable fluorescent dextrans was then loaded into the tip, followed by a covering of high-density (0.86 mg/ml) mineral oil (330760; Sigma-Aldrich) of appropriate height to generate specified hydrostatic pressures. The column was left in place for 30 min and then carefully drained and removed. Mice were then removed from the stereotaxic frame, and brains were fixed by transcardial perfusion as described above for cisternal injections.

Sample preparation and imaging
Fixed brains were cut as 100-µm coronal slices using a vibratome and imaged by confocal microscopy as described previously (Smith et al., 2017). For costaining with vascular markers, 20-µm-thick frozen sections were cut and stained with the antibodies and mounted on slides for imaging by confocal microscopy.

Image analysis
The fractional surface coverage by fluorescent solute was determined by measuring the fraction of the total fluorescently stained circumference in coronal sections. The fraction of the area labeled with fluorescent dextran was determined by gray level thresholding of each image at a fixed value, followed by division of the thresholded area by total slice area. The extent of cortical perivascular dye penetration was determined by measuring the distance of the farthest labeled vessel from the surface. The extent of parenchymal dye penetration across the pial layer was determined by measuring the intensity profile along a box perpendicular to the brain surface and measuring the distance at which fluorescence fell to half of its initial value (Smith et al., 2017). Thresholding and image measurements was done using Fiji software; graphing and statistical analysis were done with GraphPad Prism software.

Smith et al.
AQP4-independent solute uptake in brain

Journal of General Physiology
https://doi.org/10.1085/jgp.202112898

2 of 10

ICP measurement

Mice were anesthetized with ketamine and xylazine and immobilized on a stereotaxic frame. A 0.9-mm-diameter burr hole was made above the striatum, and a 1-F pressure transducer (Millar Research Products) connected to a PC recording system via an amplifier and digitizer (Biopac Systems Inc.) was lowered 1 mm into the brain and cemented in place. A 30-g needle was inserted into the cisterna magna, and aCSF was infused at specified rates using a syringe pump. Recordings were made for a 10-min baseline period, 30 min during fluid infusion, and 20 min during recovery. The average steady-state pressure elevation during the first 10 min of infusion was determined from the pressure traces.

In vivo imaging

For imaging through intact skull, mice were anesthetized and immobilized on a stereotaxic frame, and the skin overlying the skull was removed. The head was imaged with a charge-coupled device camera on a dissecting microscope at a frame rate of 0.1 Hz using reflected white light illumination. aCSF containing Evans blue (EB) dye was infused by cisternal injection at specified rates after a 10-min baseline imaging period. The change in image intensity, normalized to initial intensity, due to the presence of EB was then computed.

Online supplemental material

Raw image sequences from representative in vivo imaging experiments were annotated in Fiji and saved as video files. Conversion to MP4 format was done with multimedia software (VLC Media Player). Video 1 and Video 2 show EB dispersal at the brain surface following low- and high-volume injection, respectively.

Results

High-volume cisternal injection increases solute uptake in brain

Experimental measurements of solute uptake in brain after injection into the CSF at the cisterna magna have substantial variability (Iliff et al., 2012; Smith et al., 2017; Mestre et al., 2018a). To investigate whether the rate of cisternal fluid injection is an important determinant of parenchymal solute uptake, we first compared fixed amounts of fluorescent dextrans (10, 70, and 2,000 kD) injected slowly (5 µl at 0.5 µl/min) or diluted into a 10-fold greater volume and injected over the same time period (50 µl at 5 µl/min; Fig. 1 A, left). Greatly increased fluorescent dye staining was seen in coronal sections of brain with the high-volume fluid injection, with notably increased uptake at the dorsal surface of the brain and in deeper brain regions (Fig. 1 A, right).

Quantitative analysis of brain sections from different mice revealed fluorescence over ~90% of the brain surface with the high-volume injections (Fig. 1 B, left). Staining was substantially reduced with the low-volume injections and was not seen on the dorsal surface of the brain, indicating poor dispersal of fluorescent dyes in the subarachnoid space. To quantify fluorescent dye entry into the perivascular compartment, images were thresholded at a level where only perivascular staining was included, and the fractional fluorescently labeled area was determined (Fig. 1 B, right). The fractional-labeled area was much greater with the high-volume injection. Fluid injection at the lower rate had little effect on ICP, whereas injection at the higher rate increased ICP by ~8 mmHg (Fig. 1 C). As solutes may be rapidly cleared to lymphatics at the base of the brain (Ahn et al., 2019; Ma et al., 2019), we also investigated the effect of infusing a high volume of dye-free fluid after a low-volume dye injection. Dyes were injected slowly (5 µl at 0.5 µl/min) and then chased with either a high (50 µl at 5 µl/min) or low (5 µl at 0.5 µl/min) volume of aCSF (Fig. 1 D). The high-volume chase significantly increased fluorescent staining of brain sections, demonstrating that the dyes remained in the CSF after the low-volume injection (Fig. 1, D and E). These results demonstrate that transfer of solutes from the CSF to the brain parenchyma is highly sensitive to injection conditions.

Further studies investigated the mechanism of solute entry in brain with the high- and low-volume injections. Measurements were made in the piriform cortex, where solute accumulation was seen with both the low- and high-volume injections (Fig. 2 A). Previously, we and others reported that solute uptake in the perivascular compartment is independent of solute size, whereas parenchymal uptake is highly size dependent (Iliff et al., 2012; Smith et al., 2017), suggesting that solute transport in the parenchyma is primarily diffusive. This result was seen with the low-volume injections, in which all three dextrans penetrated comparably into the proximal perivascular compartment but penetrated in a size-dependent manner into the parenchyma (Fig. 2, A and B). For the high-volume injections, each of the solutes was again taken up in the perivascular compartment and visible around both large and small vessels, and penetration into parenchyma was size dependent. High-volume injections increased perivascular penetration of each of the three dextrans by approximately fourfold compared with low-volume injections, although penetration into parenchyma was minimally affected, with significant increase seen only for the smallest dextran. Dextran uptake under both conditions was limited to the periarterial spaces and capillaries, as accumulation was not seen in ascending cortical venules (Fig. 2 C). High-volume injection thus increases solute uptake in the perivascular compartment without altering the size dependence of uptake in the parenchyma or inducing CSF flow into the perivenular spaces.

Increased solute dispersion in the subarachnoid space following high-volume injection

As fixation may alter the distribution of labeled solutes in the CSF and brain (Ma et al., 2019), real-time brain surface imaging was done following cisternal injections of EB dye. With low-volume injections, EB appeared very slowly over the brain surface and preferentially accumulated in caudal areas, whereas with high-volume injections EB rapidly accumulated in all areas (Fig. 3 A, left panels; Video 1; and Video 2). Image intensity within circular regions along the rostrocaudal axis (normalized to relative to initial intensity; Fig. 3 A, right) revealed that high-volume injections increased both the rate at which EB appeared at
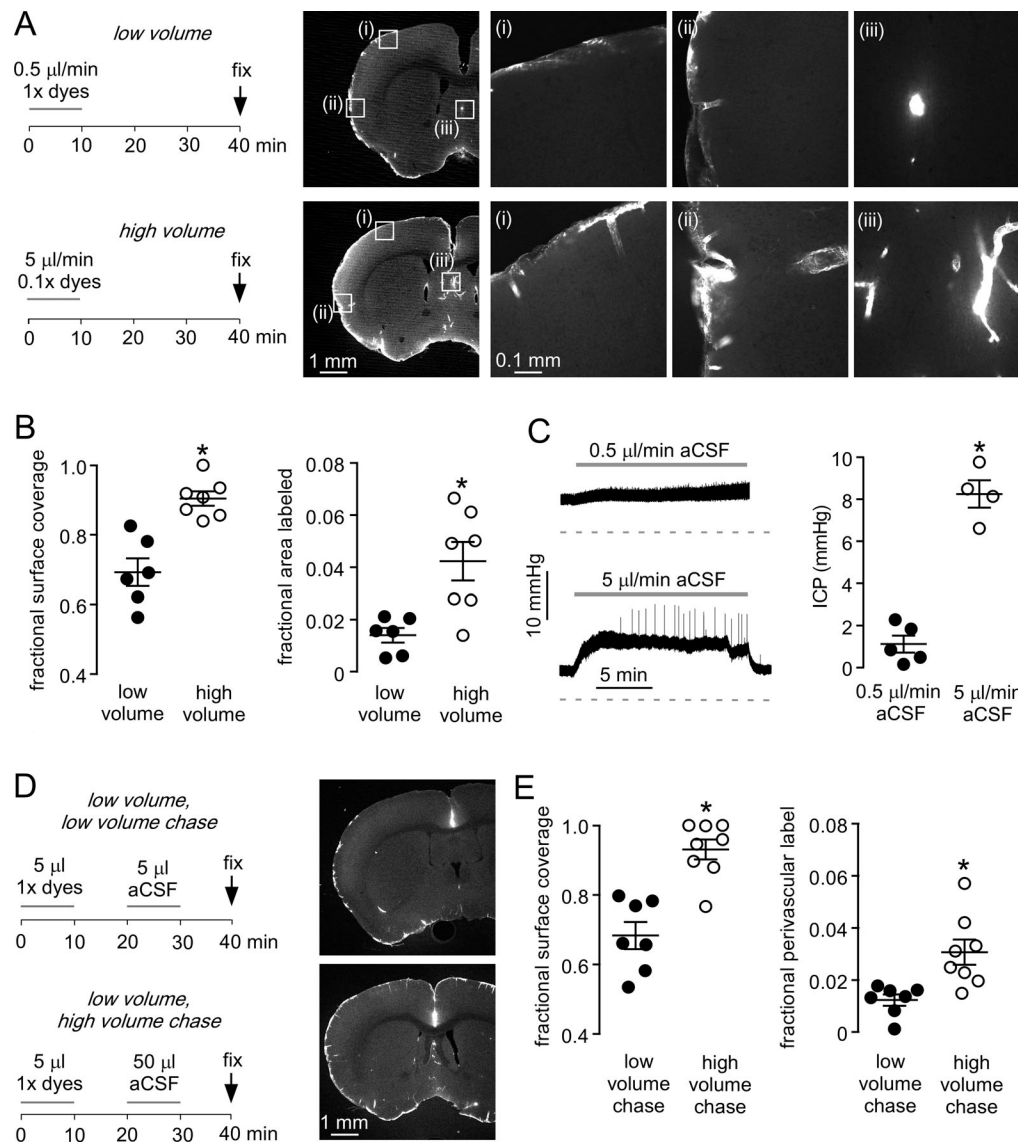
Figure 1. **Cisternal injection volume is an important determinant of solute uptake in brain. (A)** Left: Low- and high-volume injection protocols in which a fixed amount of fluorescent dextran dissolved in 5 µl (1× dye) or 50 µl (0.1× dye) of aCSF was injected over 10 min. Mice were sacrificed by perfusion fixation 30 min after injection. Right: Fluorescence images showing the distribution of 70-kD fluorescent dextran in brain sections at low resolution (left images), with higher-magnification images in the boxes marked (i)–(iii) (right images). **(B)** Left: Fraction of brain surface covered by dye ($n = 6$–7 mice; *, P = 0.0004, t test). Right: Fraction of brain area labeled with dextran (*, P = 0.0063, t test). **(C)** Left: ICP during cisternal aCSF injections at 0.5 and 5 µl/min. Right: Mean change in ICP during injections ($n = 4$–5; *, P = 0.0002, t test). **(D)** Left: Low- and high-volume chase injection protocols, with 5 µl of dye-containing solution injected over 10 min and then chased with 5 or 50 µl aCSF over 10 min. Right: Fluorescence images showing the distribution of 70-kD fluorescent dextran. **(E)** Left: Fraction of the brain surface covered by dye with low- and high-volume chase protocols ($n = 7$–8 mice; *, P = 0.0002, t test). Right: Fraction of brain area covered by dye (*, P = 0.0056, t test).

the brain surface and the peak amount of EB (Fig. 3 B). When a low-volume EB injection was followed by a high volume of aCSF (as in Fig. 1 D), EB dispersal was greatly increased by the aCSF chase (Fig. 3 C). These results are consistent with the distribution of fluorescent dextrans observed at the brain surface in fixed samples and demonstrate that dispersal of cisternally injected solutes in the CSF is highly dependent on injection conditions.

A major tenet of the glymphatic hypothesis is AQP4-dependent solute movement from CSF to brain parenchyma. Having demonstrated the effects of injection volume and the

extent of solute dispersion in the perivascular compartment as determinants of solute uptake in brain parenchyma, we re-examined the role of AQP4 in parenchymal solute uptake using high-volume cisternal injections and direct solute application. Solute uptake following high-pressure cisternal injections was similar in wild-type and AQP4 knockout mice (Fig. 4 A), with quantitative analysis showing no significant differences in either the extent to which fluorescent dextrans covered the brain surface or the area of uptake as determined by thresholding (Fig. 4 B). The extent and size dependence of fluorescent dextran accumulation in the cortical parenchyma and perivascular
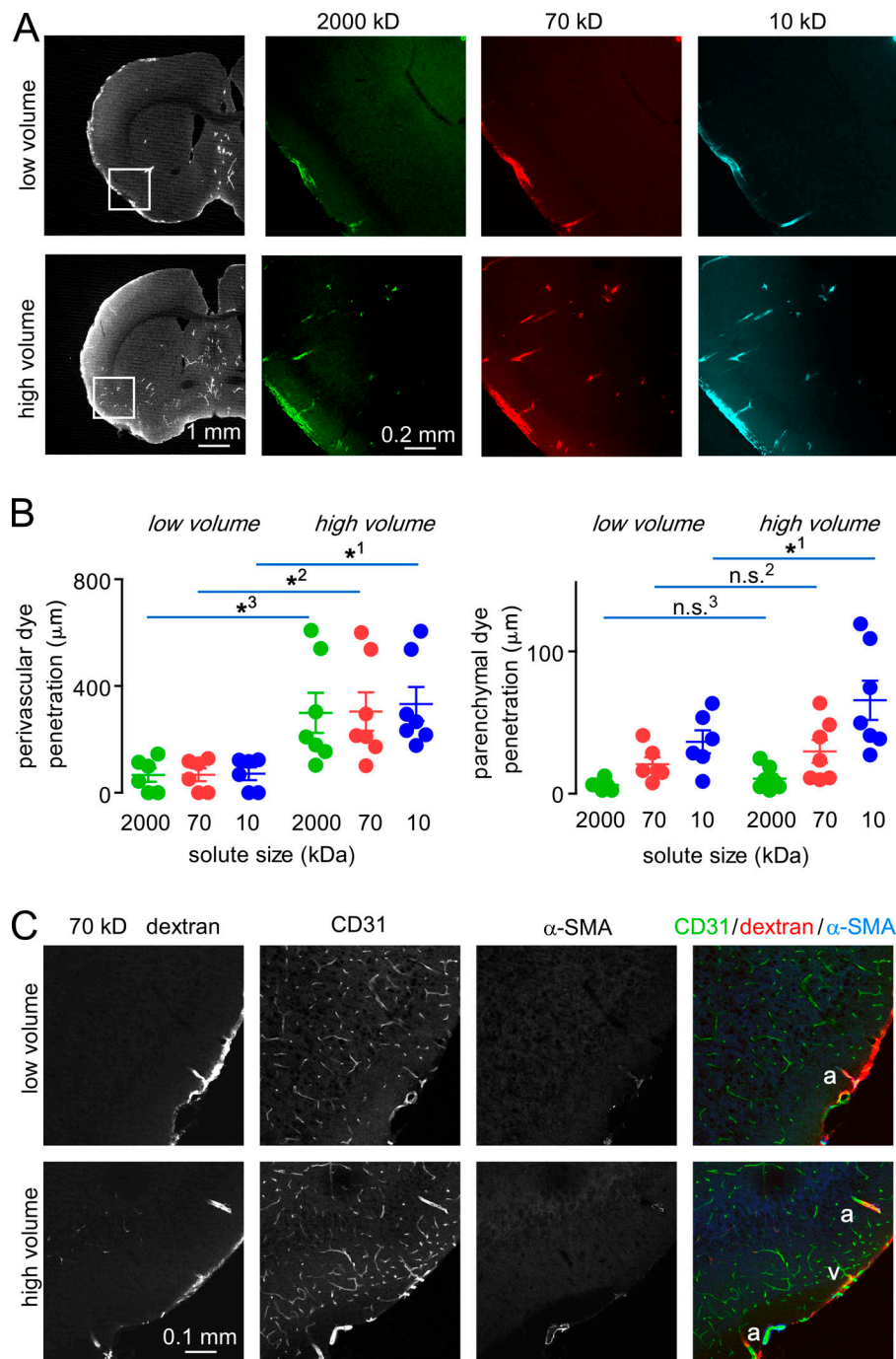
Figure 2. **Routes of fluorescent dextran entry into the brain from CSF. (A)** Left: Distribution of 70-kD dextran in brain after low- and high-volume cisternal injections. Center and right: Fluorescence images of the boxed regions at the left, showing the distribution of 2,000-kD FITC dextran, 70-kD TRITC dextran, and 10-kD Alexa Fluor 647 dextran in brain perivascular space and parenchyma. **(B)** Left: Depth of dye penetration into the perivascular spaces of cortex (n = 6 mice, *[1], P = 0.0074; *[2], P = 0.0165; *[3], P = 0.0188, repeated-measures two-way ANOVA with Bonferroni posttest). Differences with dextran size not significant. Right: Depth of dye penetration into parenchyma (*[1], P = 0.0451; n.s.[2], P > 0.999; n.s.[3], P > 0.999, repeated-measures two-way ANOVA with Bonferroni posttest). **(C)** Routes of solute uptake of cisternally injected 70-kD TRITC dextran, counterstained with CD31 (labels all vessels) and α-SMA (labels arterioles). a, descending arteriole; v, ascending venule.

compartment were also not significantly altered by AQP4 deletion.

Direct application of fluorescent dextrans to the brain surface under constant pressure

Because of the complex time-, pressure-, and location-dependent effects following cisternal solute injections, an approach was developed to continuously apply a specified concentration of solute at the brain surface at a specified pressure. After craniotomy and removal of a small area of the dura covering the cortex, a plastic pipette containing aCSF with dissolved fluorescent dextrans, with an overlying oil layer, was glued to form a watertight cylindrical reservoir over the craniotomy (Fig. 5 A). After durotomy, the pia at the brain surface was intact, without evidence of swelling or inflammation (Fig. 5 B). A small volume (300 μl) of aCSF containing fluorescent dextrans contacted the brain surface and was overlaid with a 0.5- or 30-cm column of high-density mineral oil (0.85 g/ml, equivalent to 0.3 or 18.7 mmHg) to clamp pressure.

Under the low-pressure condition, there was limited and size-dependent fluorescent dextran uptake at the brain surface, without apparent accumulation in the perivascular compartment (Fig. 5 C, top). In contrast, under the high-pressure condition, fluorescent dextran was seen in both the perivascular
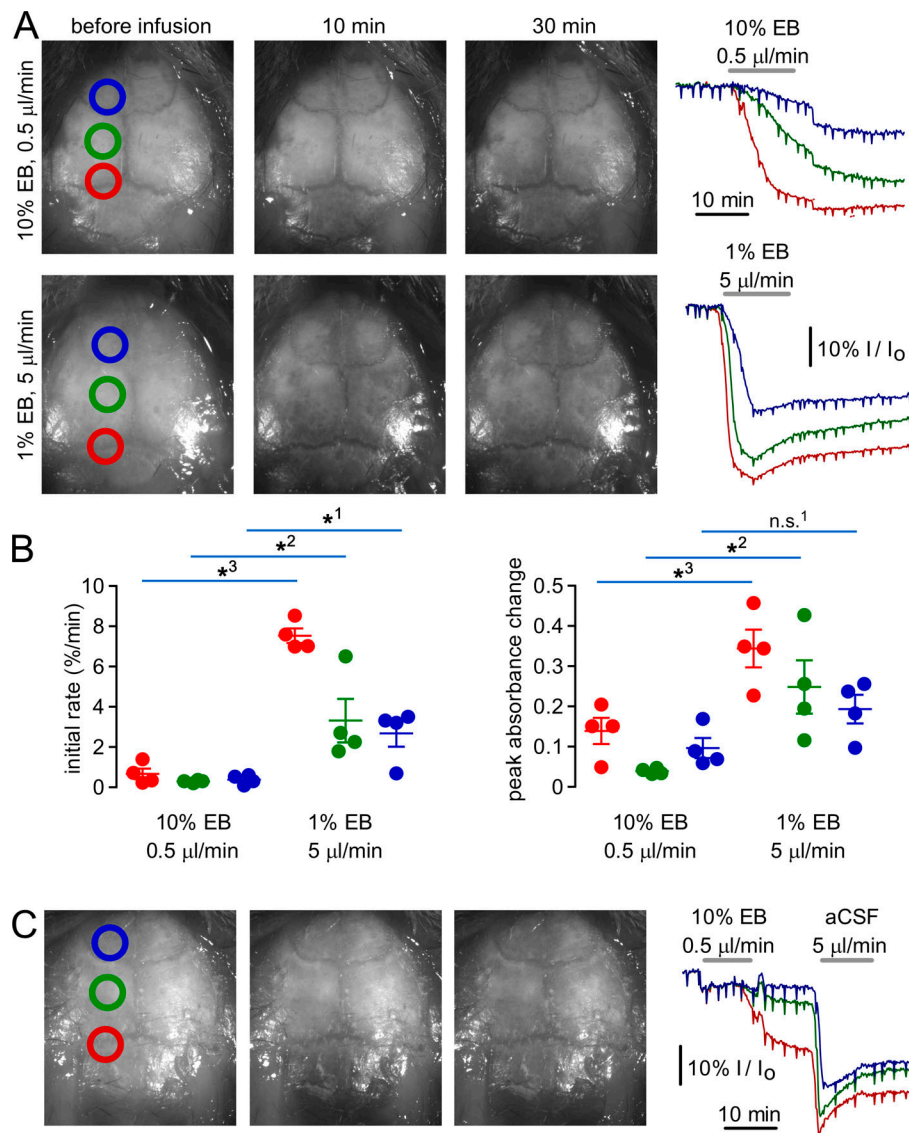
Figure 3. **Kinetics of EB distribution in the CSF subarachnoid space following high- and low-volume cisternal injections. (A)** Left: Images of the brain surface before and 10 and 30 min after cisternal injection of 50 µl of 1% EB in aCSF (high volume) or 5 µl of 10% EB in aCSF (low volume). Right: Average relative intensity (I/I_o) of pixels within the colored circles in images at the left. **(B)** Left: Initial rate of decline in I/I_o during cisternal EB infusion (*[1], P = 0.0143; *[2], P = 0.0312; *[3], P < 0.00001, t test; n = 4 mice). Right: Maximum percentile change in I/I_o during EB infusion (n.s.[1], P = 0.0678; *[2], P = 0.0193; *[3], P = 0.0115, t test; n = 4 mice). **(C)** Images of the brain surface (left) and relative intensity (right) during infusion of 5 µl of 10% EB, followed by 50 µl of aCSF.

compartment and the parenchyma (Fig. 5 C, bottom). Analysis of fluorescence as a function of distance from the brain surface showed size-dependent parenchymal dextran accumulation under both conditions (Fig. 5 D). Analysis of the extent of perivascular uptake demonstrated robust, size-independent perivascular dextran penetration under the high-pressure condition, but little perivascular uptake under the low-pressure condition (Fig. 5 E, left). Size-dependent parenchymal dye uptake was observed under both conditions, with significantly increased penetration of the 10-kD dextran under the high-pressure condition (Fig. 4 E, right). These results demonstrate that direct solute application to the brain surface can result in uptake in both parenchymal and perivascular compartments if solute is applied at sufficiently high pressure.

AQP4 deletion in mice does not affect pressure-driven fluorescent dextran accumulation in brain

Lastly, we applied fluorescent dextrans directly onto the brain surface under constant pressure to investigate the role of AQP4 on solute uptake under conditions in which dextran concentration

and pressure at the brain surface are held constant. Similar parenchymal and perivascular uptake was observed in slices prepared from wild-type and AQP4 knockout mice following direct fluorescent dextran application to the brain surface (Fig. 6 A). No significant differences were seen in the extent of parenchymal or perivascular fluorescent dextran uptake in wild-type versus AQP4 knockout mice (Fig. 6 B). These results provide further support for the conclusion that AQP4 is not required for uptake of CSF solutes in the brain.

Discussion

The original aim of this study was to identify the sources of variability in experimental studies of solute movement from CSF to ISF in brain following cisternal fluid injection. This work was motivated by the ongoing controversy over the existence of a glymphatic system in brain, whose major tenet is AQP4-dependent, advective transport of solutes into and through the ISF space. Our results suggest that the high variability of solute uptake into the interstitial space following cisternal injection is
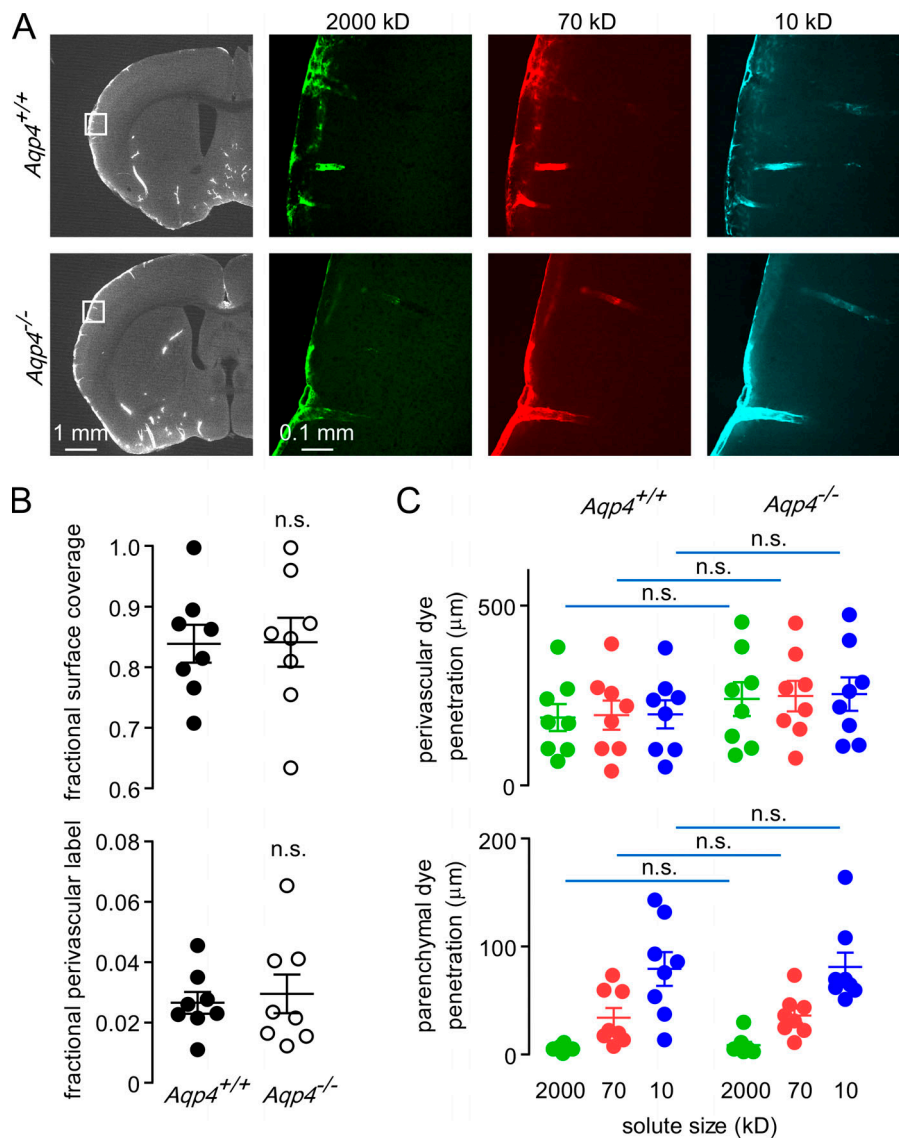
Figure 4. AQP4 deletion does not alter the distribution of fluorescent dextrans in brain following high-volume cisternal injection. (A) Left: Low-magnification images showing distribution of 70-kD dextran. Right: High-magnification images showing distribution of 2,000-, 70-, and 10-kD fluorescent dextrans in brain cortex after high-volume injection in wild-type (AQP4$^{+/+}$) and AQP4 knockout (AQP4$^{-/-}$) mice. **(B)** Top: Fraction of brain surface labeled with dextrans (eight mice per genotype; n.s., not significant, P = 0.9616, t test). Bottom: Fraction of brain covered with perivascular label after thresholding (eight mice per genotype, n.s., not significant, P = 0.6969, t test). **(C)** Distance of dye penetration in parenchyma and perivascular spaces in animals fixed 30 min after cisternal injection (differences between genotypes are not significant at P > 0.999, repeated-measures two-way ANOVA with Bonferroni posttest; n = 8 mice each).
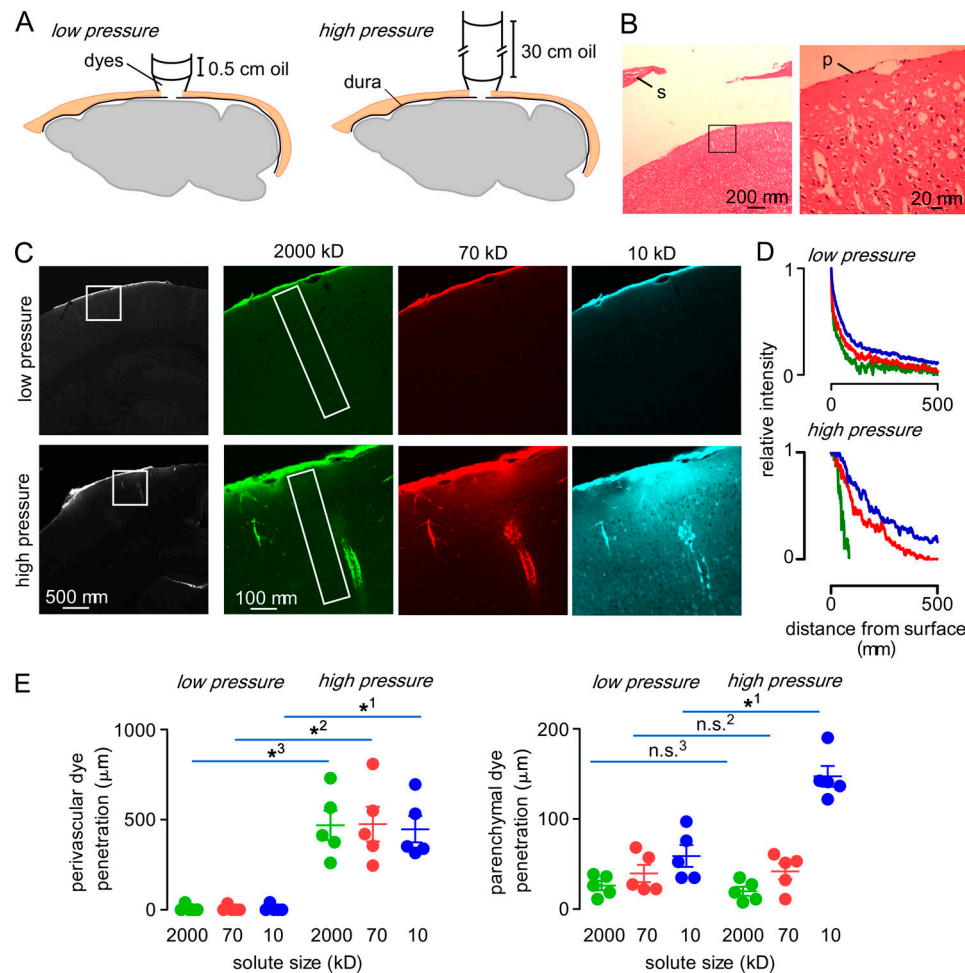
the consequence of variable solute exposure at the pial surface, which depends on injection conditions and anatomy in a complex time-, space-, and pressure-dependent manner. These findings offer an explanation for the marked variability in brain solute uptake observed following cisternal injection. To avoid the confounding sources of variability in cisternal injection experiments, we developed a constant pressure and concentration approach to investigate solute transfer from CSF to the ISF compartment. As discussed below, these experiments clarified the mechanisms of solute transport in brain and permitted direct examination of the role of AQP4 in solute transport.

We found that high injection volumes were required to effectively disperse solutes in the subarachnoid space, implying that endogenous CSF flow does not efficiently move solutes from the ventral to dorsal surfaces of the brain before they are cleared. This finding is consistent with MRI studies showing that tracers do not accumulate at the dorsal surface of mouse brain following cisternal injection (Lee et al., 2018), and with studies demonstrating enrichment of meningeal lymphatics and rapid solute clearance at the ventral surface of the mouse brain (Ahn

et al., 2019). Peristaltic solute movement around vessels in the subarachnoid space at the dorsal surface of the mouse brain has been observed and proposed to link long-range solute transport in the subarachnoid space with entry into the brain (Bedussi et al., 2018; Mestre et al., 2018b). However, this concept has been challenged on the basis that the observed transport is likely in the subarachnoid space surrounding vessels and not within the vessel wall itself (Smith and Verkman, 2019). Our findings demonstrate that significant dispersal during injection is required for solute to reach the dorsal surface of the brain, implying that paravascular peristalsis alone is not sufficient for long-range transport of solutes from the cisterna magna to the brain surface. These findings support computational and experimental studies demonstrating that high-volume injections are required for drug dispersal in the CSF and brain uptake following intrathecal injection (Tangen et al., 2017; Tangen et al., 2020), in which lower-volume injections resulted in localized drug uptake and rapid clearance to the periphery.

In addition to injection speed and volume, other experimental factors that alter CSF movement and solute dispersal

Figure 5. **Parenchymal and perivascular uptake of fluorescent dextrans applied directly to the brain surface under constant pressure conditions.** **(A)** Experimental setup in which dyes in a cylindrical pipette with overlying layer of oil contact the brain surface to clamp pressure at a specified value. **(B)** Hematoxylin and eosin staining of brain following craniotomy and durotomy. p, pia; s, skull. The enlarged subarachnoid space is a tissue-processing artifact. **(C)** Left: Distribution of 70-kD fluorescent dextran uptake in brain after 20-min application at low and high pressures. Right: Distribution of 2,000-, 70-, and 10-kD fluorescent dextrans in the boxed region at the left. **(D)** Fluorescence of each dye from the brain surface along the rectangular areas shown in C normalized to the intensity at the brain surface. **(E)** Depth of dye penetration in the perivascular and parenchymal spaces of the cortex following 30 min of direct application at low or high pressure. ([*1–3], $P < 0.001$; n.s.[2,3], $P > 0.999$, repeated-measures two-way ANOVA with Bonferroni posttest).

following injection can influence the extent of solute uptake in brain, which may explain the substantial variability in published experimental results. These factors include injection pipette tip size, consequent injection velocity, and the angle of the pipette during injection. Pulsed pressure injection, in which solute is injected in short bursts at a fixed duty cycle (Smith et al., 2017), is expected to increase solute dispersal in the CSF and uptake in the brain when compared with constant flow injection (current study). Animal posture is also an important determinant of CSF/ISF exchange (Lee et al., 2015) and additional factors, such as the use of mechanical ventilation during anesthesia, may have marked effects on dye dispersal in the subarachnoid space. It remains unclear if ICP elevation directly alters the transport of solutes from CSF to the interstitial space, as sustained pressure gradients between CSF and ISF are not observed experimentally (Penn et al., 2005); however, transient pressure differences or secondary effects of ICP elevation on vascular function might increase solute penetration in the CSF (Kedarasetti et al., 2020; Vinje et al., 2020).

As originally proposed, the glymphatic mechanism hypothesized an advective "cleansing flow" from periarterial to perivenular spaces through brain parenchyma involving AQP4-dependent fluid transport across astrocyte endfeet (Nedergaard, 2013). This mechanism was based on measurements of solute uptake in brain parenchyma following cisternal injections in four wild-type and four AQP4 knockout mice (Iliff et al., 2012). As mentioned in the Introduction, the glymphatic mechanism remains highly controversial (Hladky and Barrand, 2014; Smith and Verkman, 2018; Abbott et al., 2018), and it is now widely accepted that trans-astrocytic parenchymal convection has been largely disproven by experimental and modeling studies (Thomas, 2019; Mestre et al., 2020); however, whether AQP4 plays a role in CSF/ISF exchange remains disputed. Studies using cisternal injections to investigate the involvement of AQP4 in transporting solutes from CSF into the brain have generated remarkably variable results. Initial studies (Iliff et al., 2012) suggested that AQP4 is required for solute flow through and around endfeet following cisternal injection, but not for transport in the

A
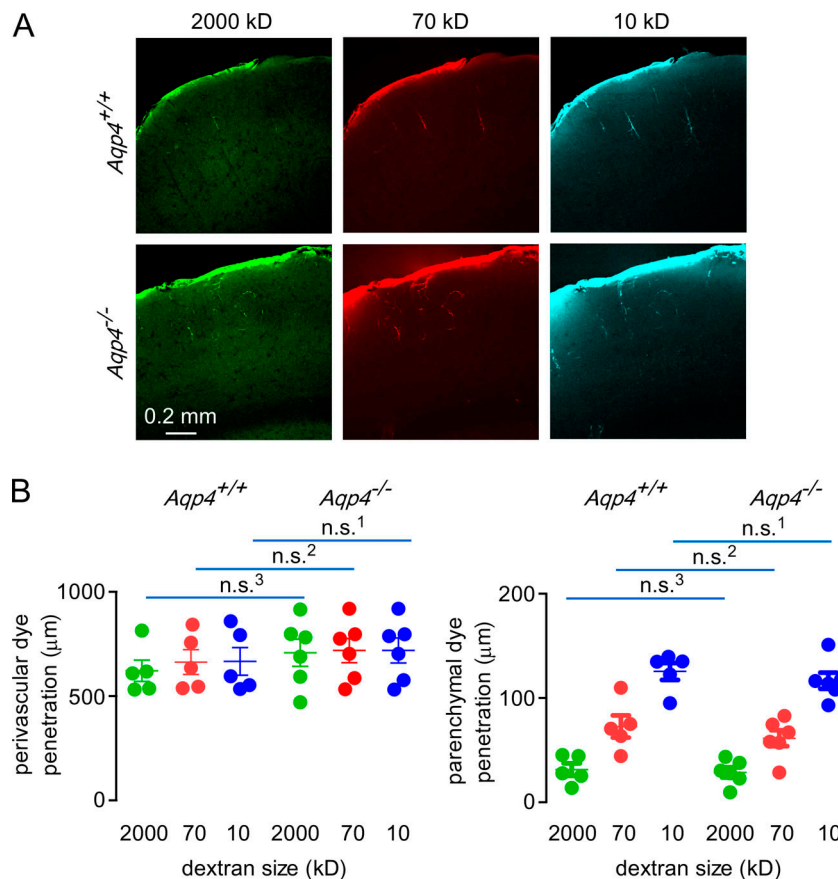
Figure 6. AQP4 deletion does not alter the distribution of fluorescent dextrans in brain following direct application under constant pressure. (A) Images showing distribution of 2,000-, 70-, and 10-kD fluorescent dextrans in brain cortex after direct surface application in wild-type and AQP4 knockout mice. **(B)** Left: Quantification of dye penetration in the perivascular spaces in mice of each genotype (n.s.[1,2], P > 0.999; n.s.[3], P = 0.986, repeated-measures two-way ANOVA with Bonferroni posttest; n = 5 AQP4^{+/+} and 6 AQP4^{−/−} mice). Right: Quantification of dye penetration in the parenchyma in mice of each genotype (n.s.[1,3], P > 0.999; n.s.[2], P = 0.922, repeated-measures two-way ANOVA with Bonferroni posttest; n = 5 AQP4^{+/+} and 6 AQP4^{−/−} mice).

B

perivascular compartment. We subsequently reported failure to detect an effect of AQP4 deletion on brain uptake of cisternally injected CSF solutes (Smith et al., 2017), which was later challenged by work from a consortium of authors reporting to have replicated the AQP4-dependent effect (Mestre et al., 2018a). Their results suggested (a) very limited parenchymal solute uptake with some sensitivity to *Aqp4* deletion (University of Rochester group, Riken group); (b) alterations in the extent of perivascular solute transport (Northern Michigan University group); (c) failure of intrathecally injected dyes to reach the cortical surface in AQP4-deficient mice (University of North Carolina group); and (d) a small effect of *Aqp4* deletion on solute penetration in the cortex (Riken group). Notably, in no case was the dramatic reduction in brain uptake of CSF solutes by AQP4 deficient mice reported by Iliff et al. (2012) reproduced. Our results suggest that the variability in basal solute uptake observed in the different laboratories may be attributed to differences in the technical details of cisternal injections.

The data here demonstrate that AQP4 is not required for parenchymal uptake of solutes from the CSF in mouse brain, even under conditions where extensive solute uptake occurs. As a caveat, we cannot exclude the possibility that water transport via AQP4 may have secondary effects on solute exchange between the CSF and ISF under different experimental conditions, for example when the injected solution is anisosmolar with respect to the ISF. Additionally, as in previous studies where the AQP4 sensitivity of parenchymal solute uptake was determined (Iliff et al., 2012; Smith et al., 2017; Mestre et al., 2018a), we have relied on bulk measurements of solute uptake in the cortex to

determine the AQP4 sensitivity of brain solute uptake, which are unable to distinguish solute transport from the perivascular spaces into the parenchyma from transport directly across the pia and glia limitans. Despite AQP4 being similarly enriched at perivascular endfeet and the glia limitans, it remains possible that AQP4 might function differently in regulating parenchymal solute uptake across these structures. In summary, our studies demonstrate that uptake of solutes in brain following cisternal injection is highly sensitive to injection conditions and consequently artifact prone, and thus not well suited to mechanistic studies.

References

Abbott, N.J. 2004. Evidence for bulk flow of brain interstitial fluid: significance for physiology and pathology. *Neurochem. Int.* 45:545–552. https://doi.org/10.1016/j.neuint.2003.11.006

Abbott, N.J., M.E. Pizzo, J.E. Preston, D. Janigro, and R.G. Thorne. 2018. The role of brain barriers in fluid movement in the CNS: is there a 'glymphatic' system? *Acta Neuropathol.* 135:387–407. https://doi.org/10.1007/s00401-018-1812-4

Ahn, J.H., H. Cho, J.H. Kim, S.H. Kim, J.S. Ham, I. Park, S.H. Suh, S.P. Hong, J.H. Song, Y.K. Hong, et al. 2019. Meningeal lymphatic vessels at the skull base drain cerebrospinal fluid. *Nature.* 572:62–66. https://doi.org/10.1038/s41586-019-1419-5

Albargothy, N.J., D.A. Johnston, M. MacGregor-Sharp, R.O. Weller, A. Verma, C.A. Hawkes, and R.O. Carare. 2018. Convective influx/glymphatic system: tracers injected into the CSF enter and leave the brain along separate periarterial basement membrane pathways. *Acta Neuropathol.* 136:139–152. https://doi.org/10.1007/s00401-018-1862-7

Bakker, E.N., B.J. Bacskai, M. Arbel-Ornath, R. Aldea, B. Bedussi, A.W. Morris, R.O. Weller, and R.O. Carare. 2016. Lymphatic clearance of the brain: perivascular, paravascular and significance for neurodegenerative diseases. *Cell. Mol. Neurobiol.* 36:181–194. https://doi.org/10.1007/s10571-015-0273-8

Bedussi, B., M. Almasian, J. de Vos, E. VanBavel, and E.N. Bakker. 2018. Paravascular spaces at the brain surface: Low resistance pathways for cerebrospinal fluid flow. *J. Cereb. Blood Flow Metab.* 38:719–726. https://doi.org/10.1177/0271678X17737984

Bedussi, B., M.G. van Lier, J.W. Bartstra, J. de Vos, M. Siebes, E. VanBavel, and E.N. Bakker. 2015. Clearance from the mouse brain by convection of interstitial fluid towards the ventricular system. *Fluids Barriers CNS.* 12:23. https://doi.org/10.1186/s12987-015-0019-5

Carare, R.O., M. Bernardes-Silva, T.A. Newman, A.M. Page, J.A. Nicoll, V.H. Perry, and R.O. Weller. 2008. Solutes, but not cells, drain from the brain parenchyma along basement membranes of capillaries and arteries: significance for cerebral amyloid angiopathy and neuroimmunology. *Neuropathol. Appl. Neurobiol.* 34:131–144. https://doi.org/10.1111/j.1365-2990.2007.00926.x

Hladky, S.B., and M.A. Barrand. 2014. Mechanisms of fluid movement into, through and out of the brain: evaluation of the evidence. *Fluids Barriers CNS.* 11:26. https://doi.org/10.1186/2045-8118-11-26

Holter, K.E., B. Kehlet, A. Devor, T.J. Sejnowski, A.M. Dale, S.W. Omholt, O.P. Ottersen, E.A. Nagelhus, K.A. Mardal, and K.H. Pettersen. 2017. Interstitial solute transport in 3D reconstructed neuropil occurs by diffusion rather than bulk flow. *Proc. Natl. Acad. Sci. USA.* 114:9894–9899. https://doi.org/10.1073/pnas.1706942114

Ichimura, T., P.A. Fraser, and H.F. Cserr. 1991. Distribution of extracellular tracers in perivascular spaces of the rat brain. *Brain Res.* 545:103–113. https://doi.org/10.1016/0006-8993(91)91275-6

Iliff, J.J., M. Wang, Y. Liao, B.A. Plogg, W. Peng, G.A. Gundersen, H. Benveniste, G.E. Vates, R. Deane, S.A. Goldman, et al. 2012. A paravascular pathway facilitates CSF flow through the brain parenchyma and the clearance of interstitial solutes, including amyloid β. *Sci. Transl. Med.* 4:147ra111. https://doi.org/10.1126/scitranslmed.3003748

Jin, B.J., A.J. Smith, and A.S. Verkman. 2016. Spatial model of convective solute transport in brain extracellular space does not support a "glymphatic" mechanism. *J. Gen. Physiol.* 148:489–501. https://doi.org/10.1085/jgp.201611684

Kedarasetti, R.T., P.J. Drew, and F. Costanzo. 2020. Arterial pulsations drive oscillatory flow of CSF but not directional pumping. *Sci. Rep.* 10:10102. https://doi.org/10.1038/s41598-020-66887-w

Kutuzov, N., H. Flyvbjerg, and M. Lauritzen. 2018. Contributions of the glycocalyx, endothelium, and extravascular compartment to the blood-brain barrier. *Proc. Natl. Acad. Sci. USA.* 115:E9429–E9438. https://doi.org/10.1073/pnas.1802155115

Lee, H., K. Mortensen, S. Sanggaard, P. Koch, H. Brunner, B. Quistorff, M. Nedergaard, and H. Benveniste. 2018. Quantitative Gd-DOTA uptake from cerebrospinal fluid into rat brain using 3D VFA-SPGR at 9.4T. *Magn. Reson. Med.* 79:1568–1578. https://doi.org/10.1002/mrm.26779

Lee, H., L. Xie, M. Yu, H. Kang, T. Feng, R. Deane, J. Logan, M. Nedergaard, and H. Benveniste. 2015. The effect of body posture on brain glymphatic transport. *J. Neurosci.* 35:11034–11044. https://doi.org/10.1523/JNEUROSCI.1625-15.2015

Ma, Q., M. Ries, Y. Decker, A. Müller, C. Riner, A. Bücker, K. Fassbender, M. Detmar, and S.T. Proulx. 2019. Rapid lymphatic efflux limits cerebrospinal fluid flow to the brain. *Acta Neuropathol.* 137:151–165. https://doi.org/10.1007/s00401-018-1916-x

Ma, T., B. Yang, A. Gillespie, E.J. Carlson, C.J. Epstein, and A.S. Verkman. 1997. Generation and phenotype of a transgenic knockout mouse lacking the mercurial-insensitive water channel aquaporin-4. *J. Clin. Invest.* 100:957–962. https://doi.org/10.1172/JCI231

Manley, G.T., M. Fujimura, T. Ma, N. Noshita, F. Filiz, A.W. Bollen, P. Chan, and A.S. Verkman. 2000. Aquaporin-4 deletion in mice reduces brain edema after acute water intoxication and ischemic stroke. *Nat. Med.* 6:159–163. https://doi.org/10.1038/72256

Mestre, H., L.M. Hablitz, A.L. Xavier, W. Feng, W. Zou, T. Pu, H. Monai, G. Murlidharan, R.M. Castellanos Rivera, M.J. Simon, et al. 2018a. Aquaporin-4-dependent glymphatic solute transport in the rodent brain. *eLife.* 7:e40070. https://doi.org/10.7554/eLife.40070

Mestre, H., J. Tithof, T. Du, W. Song, W. Peng, A.M. Sweeney, G. Olveda, J.H. Thomas, M. Nedergaard, and D.H. Kelley. 2018b. Flow of cerebrospinal fluid is driven by arterial pulsations and is reduced in hypertension. *Nat. Commun.* 9:4878. https://doi.org/10.1038/s41467-018-07318-3

Mestre, H., Y. Mori, and M. Nedergaard. 2020. The brain's glymphatic system: Current controversies. *Trends Neurosci.* 43:458–466. https://doi.org/10.1016/j.tins.2020.04.003

Nedergaard, M. 2013. Neuroscience. Garbage truck of the brain. *Science.* 340:1529–1530. https://doi.org/10.1126/science.1240514

Penn, R.D., M.C. Lee, A.A. Linninger, K. Miesel, S.N. Lu, and L. Stylos. 2005. Pressure gradients in the brain in an experimental model of hydrocephalus. *J. Neurosurg.* 102:1069–1075. https://doi.org/10.3171/jns.2005.102.6.1069

Pizzo, M.E., D.J. Wolak, N.N. Kumar, E. Brunette, C.L. Brunnquell, M.J. Hannocks, N.J. Abbott, M.E. Meyerand, L. Sorokin, D.B. Stanimirovic, and R.G. Thorne. 2018. Intrathecal antibody distribution in the rat brain: surface diffusion, perivascular transport and osmotic enhancement of delivery. *J. Physiol.* 596:445–475. https://doi.org/10.1113/JP275105

Rash, J.E., T. Yasumura, C.S. Hudson, P. Agre, and S. Nielsen. 1998. Direct immunogold labeling of aquaporin-4 in square arrays of astrocyte and ependymocyte plasma membranes in rat brain and spinal cord. *Proc. Natl. Acad. Sci. USA.* 95:11981–11986. https://doi.org/10.1073/pnas.95.20.11981

Rosenberg, G.A., W.T. Kyner, and E. Estrada. 1980. Bulk flow of brain interstitial fluid under normal and hyperosmolar conditions. *Am. J. Physiol.* 238:F42–F49. https://doi.org/10.1152/ajprenal.1980.238.1.F42

Smith, A.J., and A.S. Verkman. 2018. The "glymphatic" mechanism for solute clearance in Alzheimer's disease: game changer or unproven speculation? *FASEB J.* 32:543–551. https://doi.org/10.1096/fj.201700999

Smith, A.J., and A.S. Verkman. 2019. CrossTalk opposing view: Going against the flow: interstitial solute transport in brain is diffusive and aquaporin-4 independent. *J. Physiol.* 597:4421–4424. https://doi.org/10.1113/JP277636

Smith, A.J., X. Yao, J.A. Dix, B.J. Jin, and A.S. Verkman. 2017. Test of the 'glymphatic' hypothesis demonstrates diffusive and aquaporin-4-independent solute transport in rodent brain parenchyma. *eLife.* 6:e27679. https://doi.org/10.7554/eLife.27679

Syková, E., and C. Nicholson. 2008. Diffusion in brain extracellular space. *Physiol. Rev.* 88:1277–1340. https://doi.org/10.1152/physrev.00027.2007

Tangen, K., I. Nestorov, A. Verma, J. Sullivan, R.W. Holt, and A.A. Linninger. 2020. In vivo intrathecal tracer dispersion in Cynomolgus monkey validates wide biodistribution along neuraxis. *IEEE Trans. Biomed. Eng.* 67:1122–1132. https://doi.org/10.1109/TBME.2019.2930451

Tangen, K.M., R. Leval, A.I. Mehta, and A.A. Linninger. 2017. Computational and in vitro experimental investigation of intrathecal drug distribution: Parametric study of the effect of injection volume, cerebrospinal fluid pulsatility, and drug uptake. *Anesth. Analg.* 124:1686–1696. https://doi.org/10.1213/ANE.0000000000002011

Thomas, J.H. 2019. Fluid dynamics of cerebrospinal fluid flow in perivascular spaces. *J. R. Soc. Interface.* 16:20190572. https://doi.org/10.1098/rsif.2019.0572

Verbavatz, J.M., T. Ma, R. Gobin, and A.S. Verkman. 1997. Absence of orthogonal arrays in kidney, brain and muscle from transgenic knockout mice lacking water channel aquaporin-4. *J. Cell Sci.* 110:2855–2860. https://doi.org/10.1242/jcs.110.22.2855

Vinje, V., A. Eklund, K.A. Mardal, M.E. Rognes, and K.H. Støverud. 2020. Intracranial pressure elevation alters CSF clearance pathways. *Fluids Barriers CNS.* 17:29. https://doi.org/10.1186/s12987-020-00189-1

Zervas, N.T., T.M. Liszczak, M.R. Mayberg, and P.M. Black. 1982. Cerebrospinal fluid may nourish cerebral vessels through pathways in the adventitia that may be analogous to systemic vasa vasorum. *J. Neurosurg.* 56:475–481. https://doi.org/10.3171/jns.1982.56.4.0475

Supplemental material

Video 1.   **Imaging of EB dispersal at the brain surface following low-volume injection (10% EB at 0.5 µl/min).** Imaging was at 0.1 Hz for 45 min. Cisternal injection was from 5 to 15 min. Videos were accelerated to 27 frames/s.

Video 2.   **Imaging of EB dispersal at the brain surface following high-volume injection (1% EB at 5 µl/min).** Imaging was at 0.1 Hz for 45 min. Cisternal injection was from 5 to 15 min. Videos were accelerated to 27 frames/s.